Growth of ZnO Nanostructures with Controllable Morphology Using a Facile Green Antisolvent Method

ARTICLE *in* THE JOURNAL OF PHYSICAL CHEMISTRY C · APRIL 2010

Impact Factor: 4.77 · DOI: 10.1021/jp102396f

4 AUTHORS, INCLUDING:

David Shan Hill Wong
National Tsing Hua University
150 PUBLICATIONS **2,530** CITATIONS

SEE PROFILE

Shih-Yuan Lu
National Tsing Hua University
159 PUBLICATIONS **3,074** CITATIONS

SEE PROFILE

CrystEngComm

Cite this: *CrystEngComm*, 2011, **13**, 6218

www.rsc.org/crystengcomm

PAPER

Ultrafast formation of ZnO mesocrystals with excellent photocatalytic activities by a facile Tris-assisted antisolvent process†

Ji-Yao Dong,[a] Wei-Hao Lin,[b] Yung-Jung Hsu,[b] David Shan-Hill Wong*[a] and Shih-Yuan Lu*[a]

Received 16th April 2011, Accepted 20th July 2011
DOI: 10.1039/c1ce05503h

Ultrafast formation of ZnO mesocrystals was achieved with a facile, green, Tris-assisted, room temperature ionic liquid based antisolvent process. A deep eutectic solvent, formed by simply mixing and heating urea and choline chloride at 70 °C, served as the solvent for ZnO, whereas Tris-containing de-ionized water acted as the anti-solvent to trigger the ultrafast formation of ZnO mesocrystals at 70 °C. The product mesocrystals were mesoporous and near-single-crystalline with high specific surface areas, showing excellent photocatalytic activities toward photodegradation of methylene blue, comparable to that of a commercial photocatalyst, P-25 TiO_2, which is rarely achieved for pristine ZnO. The present approach is a general one and can be readily extended to production of mesocrystals of other functional metal oxides.

1. Introduction

Mesocrystals, a new class of materials, have attracted considerable research attention in recent years because of their unique morphological and crystallographic structures that may enable new materials applications.[1] These nonclassical crystals are 3-dimensional (3D) superstructures composed of nanocrystal building blocks assembled in a crystallographically oriented manner. Pores of mesoscopic scale are often generated during the mesocrystallization process. This unique material form of mesoporous, near-single-crystalline particle would prove advantageous in applications requiring high specific surface areas, easy mass transfer within the pores, well-connected 3D charge transport paths, and highly oriented single crystallinity, for example, photocatalysts, electrode materials for lithium ion batteries and supercapacitors, materials for photocatalytic water splitting, to name just a few. Till now, there have been developed a wide variety of mesocrystals, including inorganic salts,[2,3] organic molecules,[4,5] metals,[6,7] and metal oxides,[8,9] whose preparations, particularly for functional metal oxides, often require chemical reactions of long reaction times and high temperatures.

In this work, we developed an/a ultrafast, facile, green, ionic liquid based, small-molecule-assisted antisolvent process for production of ZnO mesocrystals of excellent photocatalytic activities. All chemicals involved, including solutes, solvents, and additives, were environmentally friendly, and the processing temperature was low and the products were formed almost instantaneously. Here, a new class of room temperature ionic liquids, known as deep eutectic solvents (DESs), prepared by simply mixing quaternary ammonium salts with hydrogen-bond donors at temperatures often lower than 100 °C, was used as the solvent. These DESs are good solvents for metal oxides.[10] The constituents of these DESs are cheap and environmentally friendly, unlike the more traditional room temperature ionic liquids often are expensive with uncertain bio-compatibility, and highly soluble in common solvents such as water, in which metal oxides are not soluble. Therefore when metal oxide containing DES solutions are injected into a common solvent, the oxide can be readily precipitated.

We demonstrated in recent work that, by controlling the injection time and the antisolvent composition, ZnO nanostructures of controllable shape and size can be obtained.[11] In this work, we further developed a small molecule-assisted antisolvent process for ultrafast formation of ZnO mesocrystals. Here, a small molecule additive, tris(hydroxymethyl)aminomethane (Tris), of desired amounts was added into water to make the antisolvent, and commercial ZnO powders were dissolved in a DES, urea–choline chloride (UCC), to serve as the raw material. With the introduction of Tris, a rapid injection of the DES solution into the antisolvent at 70 °C produced almost instantaneously mesocrystals of ZnO. These ZnO mesocrystals were further shown to possess excellent photocatalytic activities toward photodegradation of methylene blue, comparable to that of a commercial photocatalyst, P-25 TiO_2.

[a]*Department of Chemical Engineering, National Tsing Hua University, Hsinchu, Taiwan, 30013, Republic of China. E-mail: sylu@mx.nthu.edu.tw; Fax: +886 3-5715408; Tel: +886 3-5714364; dshwong@che.nthu.edu.tw*
[b]*Department of Materials Science and Engineering, National Chiao Tung University, Hsinchu, Taiwan, 30010, Republic of China*
† Electronic supplementary information (ESI) available: SEM image. See DOI: 10.1039/c1ce05503h

2. Experimental

Preparation of ZnO-containing DES

All chemicals were used without further purification. The detailed procedures for preparation of ZnO-containing DES solutions have been described in our previous work.[11] Briefly, DES was first prepared by mixing urea and choline chloride at a 2 : 1 molar ratio in argon atmosphere (denoted as UCC). An amount of 3.6 g of ZnO powders was then added to UCC to afford a solution containing 24 000 ppm of ZnO. The UCC solution was kept in an oven at 70 °C for several days until all ZnO powders dissolved and a clear solution was obtained.

Growth of ZnO mesocrystals from an antisolvent process

Suitable amounts of Tris ($(HOCH_2)_3CNH_2$) were mixed with de-ionized water to prepare the antisolvents of different Tris concentrations (0, 5, 10, 25, 100, 500 mM) for precipitation of ZnO from the ZnO-containing DES solution. For formation of ZnO mesocrystals, 10.0 g of ZnO-containing DES were injected into 200 mL of antisolvent in 5 s in a water bath maintained at 70 °C, followed by vigorous stirring for 5 min. The resultant white suspending solids were collected by centrifugation at 6500 rpm for 30 min and washed with de-ionized water and ethanol to remove remaining DES and impurities. The product was then dispersed in ethanol for later use.

Photocatalytic performance measurement

The photocatalytic performance of ZnO mesocrystals was evaluated by the photodegradation of methylene blue (MB) under UV illumination. A quartz tube with a capacity of 30 mL was used as the reactor. The optical system used for the photocatalytic reaction was composed of a UV lamp (500 W) with a light intensity of 175 mW cm^{-2}. All photocatalysis experiments were conducted at room temperature. In a typical run, 4.0 mg of photocatalyst were added into 20 mL of MB solution (1×10^{-5} M) in the reactor. Prior to irradiation, the suspension was stirred in the dark for 60 min to reach the adsorption equilibrium between the MB and photocatalyst. At certain time intervals of irradiation, 1.0 mL of the reaction solution was withdrawn and centrifuged to remove the photocatalyst particles. The filtrates were analyzed with a UV-visible spectrophotometer to measure the concentration variation of MB through recording the corresponding absorbance of the characteristic peak of 665 nm. The concentration of MB as a function of the irradiation time was recorded to investigate the reaction kinetics of the photodegradation of MB. The concentration decay curves were then fitted to a pseudo-first-order model, from which the apparent specific rate constant (k_{MB}) was determined. To take into account the effect of the total surface area of the photocatalyst, the apparent specific rate constants were further normalized with the specific surface areas of the photocatalyst (k'_{MB}).

Characterizations

The morphology and dimensions of the products were examined with a field-emission scanning electron microscope (FESEM, Hitachi, S-4700). The crystallographic structure of the samples was investigated with an X-ray diffractometer (XRD, Rigaku, Ultima IV) and a high-resolution transmission electron microscope (HRTEM, JEOL, JEM-3000F) operated at 300 kV. Brunauer–Emmett–Teller (BET) specific surface areas and Barret–Joyner–Halenda (BJH) pore volumes of the samples were determined from the N_2 adsorption/desorption isotherms. UV-visible spectra were collected with a Hitachi U-3900H at room temperature under ambient atmosphere.

3. Results and discussion

Fig. 1 shows the SEM images and XRD patterns of products obtained at increasing concentrations of Tris. When Tris was absent from the antisolvent, the spaghetti-like structure with a large quantity of interlacing nanowires embedded in an amorphous matrix was produced. These nanowires were with diameters of 10–40 nm and lengths of hundreds of nm to several μm. When Tris of 10 mM was applied, elongated particles with rough surfaces were formed as shown in Fig. 1(b). These elongated, rough-surface particles were with a size of 100–300 nm and if examined closely they were aggregates of nanoparticles of sizes of 20–30 nm. The sizes of the nanoparticle aggregates increased

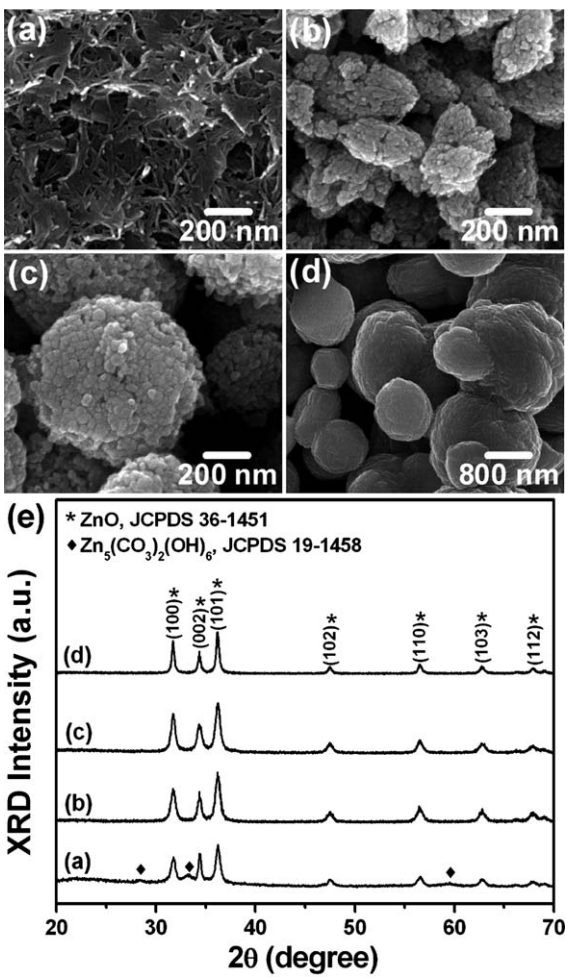

Fig. 1 SEM images of ZnO products obtained at increasing concentrations of Tris: (a) 0, (b) 10, (c) 100, (d) 500 mM. The corresponding XRD patterns are shown in (e).

to 200–800 nm with increasing the Tris concentration to 100 mM, accompanied by reduction in shape anisotropy. Further increasing the Tris concentration to 500 mM led to the formation of nanoparticle aggregates of even larger sizes (0.5–2.0 μm) but with much smoother surfaces.

The corresponding XRD patterns are presented in Fig. 1(e). All the products exhibited the crystallographic phase of wurtzite ZnO (JCPDS 36-1451). In addition to the ZnO pattern, three minor but non-negligible diffraction peaks were observed for products obtained from the Tris-absent case. The three peaks can be assigned to zinc carbonate hydroxide (JCPDS 19-1458) which resulted from the reaction of urea with Zn^{2+} during the anti-solvent process.[12]

A close examination of the XRD patterns further revealed an interesting phenomenon associated with the relative peak intensity of (002). The relative peak intensity of (002) decreased with increasing Tris concentration. This implies that there exists preferential anisotropic crystal growth along [001], the *c*-axis, of wurtzite ZnO when Tris is absent from the antisolvent, and this anisotropic crystal growth habit is retarded with the addition of Tris. To gain more insights on this interesting phenomenon, TEM and selected area electron diffraction (SAED) characterizations were conducted and the results are shown in Fig. 2. Fig. 2(a) shows a typical TEM image for the product obtained from the Tris-absent case. The nanowires appear to be distributed in an amorphous phase and the SAED shows a polycrystal ring pattern because of the random orientation of the nanowires. As for the Tris-added cases, dot patterns were obtained for the SAED. These dot patterns however were stretched for products obtained from low Tris concentration cases. The extent of dot stretching diminished with increasing Tris concentration, indicating that better single-crystallinity was acquired at higher Tris concentrations. Interestingly, the elongation direction of the nanoparticle aggregates coincided with the preferential anisotropic crystal growth direction of [001], the *c*-axis. The porous nature of the aggregates was evident from the TEM/HRTEM images, and was characterized with the N_2 adsorption/desorption isotherms.

A typical N_2 adsorption/desorption isotherm is shown in Fig. 3 for illustration. All samples exhibited type IV isotherms with type H3 hysteresis loops, typical of mesoporous materials. The BET specific surface areas were determined to be 52.4, 43.0, and 15.7 $m^2\ g^{-1}$ and the BJH pore volumes to be 0.248, 0.139, and 0.057 $cm^3\ g^{-1}$ for Tris concentrations of 10, 25, and 500 mM, respectively. Evidently, the porous aggregates became more compact in the structure with increasing Tris concentration. The SAED patterns together with the structural data derived from the N_2 adsorption/desorption isotherms indicated that the nanoparticle aggregates obtained by the present antisolvent process were ZnO mesocrystals.

Evidently, the presence of Tris molecules led to the assembly of primary nanocrystals in a crystallographically oriented manner to form the final mesocrystals. This delicate assembly process is termed "oriented attachment" (OA) and is widely documented in the literature concerning the formation of mesocrystals.[1] The so-called oriented attachment describes a spontaneous self-assembly process of adjacent nanocrystals sharing a common crystallographic orientation, eventually leading to formation of mesocrystals exhibiting near-single-crystallinity. Tris in fact has been

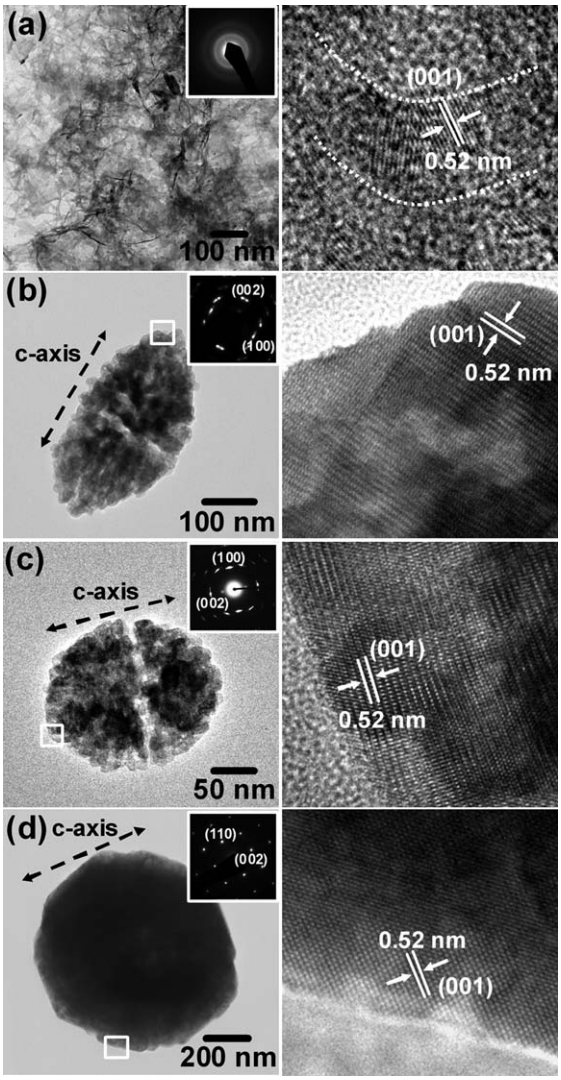

Fig. 2 TEM images, SAED patterns, and the corresponding HRTEM images for ZnO products obtained with different concentrations of Tris: (a) 0, (b) 10, (c) 25, (d) 500 mM. The edges of a constituent nanowire in (a) are highlighted with dotted lines.

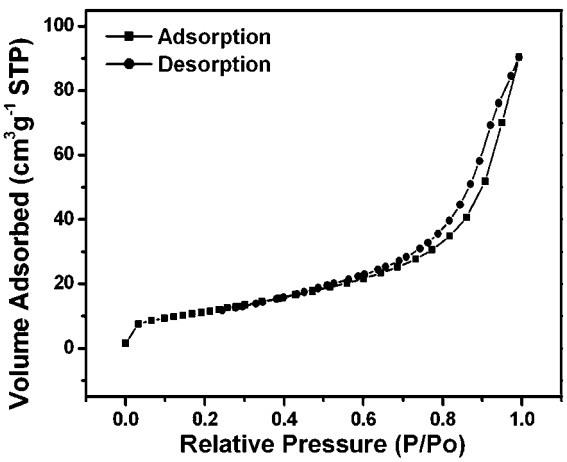

Fig. 3 N_2 Adsorption/desorption isotherm for ZnO mesocrystals obtained with a Tris concentration of 25 mM.

used as an assembler reagent to induce anisotropic assembly of TiO_2 nanocrystals prepared from precursor $TiCl_4$ beforehand.[8] As a polydentate ligand, Tris provides three OH groups binding to the TiO_2 surface and one NH_2 group pointing outward to stabilize the TiO_2 nanocrystals in protic solvents like water. It was suggested that the anisotropic assembly of TiO_2 nanocrystals was initiated by the selective removal of Tris from the (001) facets of the nanocrystals which have the highest surface energy. As a consequence of minimization of the total surface energy, preferred attachment of TiO_2 nanocrystals along the [001] direction then proceeded, leading to the formation of pearl-necklace aggregates.[8]

For the present system, the Tris molecules played the same role as an assembler reagent to facilitate formation of ZnO mesocrystals. A plausible formation mechanism for the present ZnO mesocrystals is proposed as follows. First, one notes that, in the absence of Tris, the classical anisotropic crystal growth of ZnO occurred in the antisolvent process, giving rise to the growth of nanowires along the most favorable direction, the *c*-axis. Since no assembler reagents were provided, the nanowires thus obtained were randomly entangled, resulting in the formation of the spaghetti-like structure as observed. However, with the introduction of 5 mM Tris (Fig. S1†), nanocrystal aggregates composed of isotropically shaped primary nanocrystals were generated among the spaghetti structure. This phenomenon implies a transition of crystal growth habit of ZnO from classical anisotropic crystal growth to nonclassical OA of nanocrystals upon the introduction of Tris. Further increase of Tris concentration to 10 mM resulted in mesocrystal only products (Fig. 1(b)).

Based on the above observations, we further propose that the Tris molecules bind non-specifically to every crystal facet of ZnO to inhibit anisotropic crystal growth, thus giving isotropically shaped primary nanocrystals for subsequent OA to form final mesocrystals. Although the OA of nanocrystals can proceed *via* all crystal facets of the primary nanocrystal, OA along the *c*-axis may be preferred since the *c*-planes possess the highest surface energy, removal of which leads to lower total surface energies. This OA preference in the *c*-axis will be more pronounced at low Tris concentrations. The reason is as follows. The presence of fewer Tris molecules in the system means weaker OA driving forces, and thus the energy advantage of the *c*-planes becomes more dominant. On the other hand, at high Tris concentrations, the abundant supply of Tris molecules makes it easy to proceed with OA in all crystal facets and thus the energy advantage of the *c*-planes will not stand out. In line with this logic, one expects the resulting mesocrystals to be more porous in the internal structure and more elongated along the *c*-axis in shape. In fact, the coincidence of the *c*-axis direction of the constituent nanocrystal of a mesocrystal with the elongation direction of the mesocrystal implies the preferred OA along the *c*-axis. This is what we have observed from Fig. 1 and the structural data derived from the N_2 adsorption/desorption isotherms. Furthermore, the OA preference along the *c*-axis leads to more extended crystal domain along the *c*-axis and thus the more intense diffraction peak of (002) as observed from the XRD patterns for low Tris concentration cases. In addition, weaker OA driving forces give rise to less perfect crystallographic alignment of the joining nanocrystals, and thus more stretched dots in the SAED patterns as

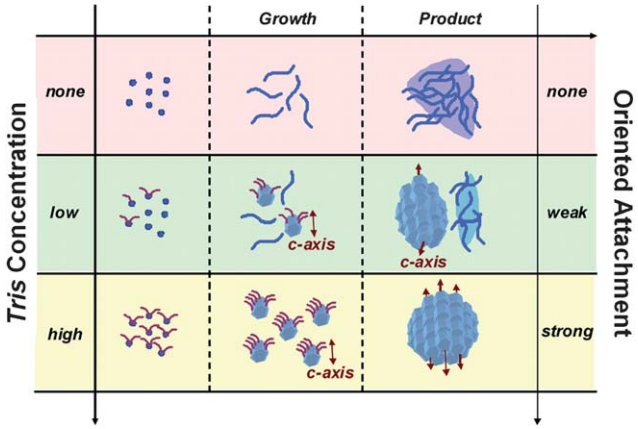

Fig. 4 Schematic illustration of the influence of the Tris additive in antisolvent on the morphology of the resulting ZnO.

evident from Fig. 2. To summarize the proposed growth mechanism, a scheme is shown in Fig. 4 to illustrate the role of the Tris additive in the formation of ZnO mesocrystals by the present antisolvent process.

The unique morphological and crystallographic structures of the present ZnO mesocrystals, including being mesoporous with high specific surface areas and pore volumes, having single crystalline nanoparticles as the building blocks, and possessing a well-connected 3D network structure, may prove advantageous in photocatalysis. We characterized their photocatalytic activities with photodegradation of MB. The results together with the structural data derived from the N_2 adsorption/desorption isotherms are summarized in Table 1. Fig. 5 shows the normalized MB concentration as a function of the irradiation time for samples prepared at the Tris concentrations of 25, 100, and 500 mM. Also included in the figure is the concentration decay curve for P-25 TiO_2. As expected, the photodegradation proceeded the fastest for the P-25 sample. The performances of samples 25 and 100 mM however do not lag too far behind from that of sample P-25.

Here, the specific rate constants determined from Fig. 5 were taken as the quantitative measure for the photocatalytic activity. Evidently, from Table 1, the photocatalytic activity decreased with increasing Tris concentration, with the product from 25 mM of Tris achieving the highest level among the three mesocrystal samples, but still lagging behind that of P-25 TiO_2. This trend correlates well with the magnitudes of the specific surface area and pore volume, which is expected since higher surface areas

Table 1 Specific surface areas, pore volumes, apparent photocatalytic specific rate constants (k_{MB}), and specific surface area normalized photocatalytic specific rate constants (k'_{MB}) for ZnO mesocrystals obtained at different concentrations of Tris and a commercial photocatalyst, P-25 TiO_2

Tris concentration/mM	Surface area/m^2 g^{-1}	Pore volume/cm^3 g^{-1}	k_{MB}/h^{-1} g^{-1}	k'_{MB}/h^{-1} m^{-2}
25	43.0	0.139	1074	25.0
100	29.6	0.119	839	28.3
500	15.7	0.057	123	7.8
P-25 TiO_2	70.8	0.226	2048	28.9

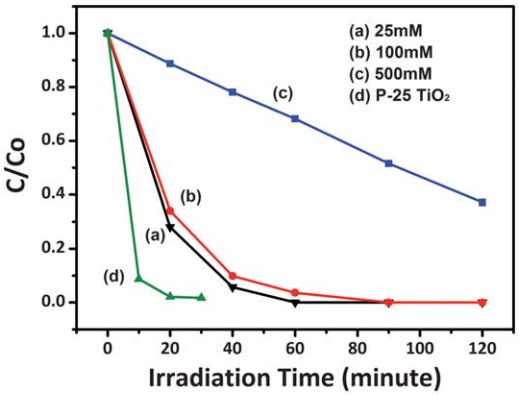

Fig. 5 Normalized concentration decay *vs.* irradiation time curves for samples prepared at Tris concentrations of 25, 100, and 500 mM and sample P-25 TiO_2.

offer more active sites for photocatalytic reactions and higher pore volumes ease the mass transfer of participant species in and out of the porous structure. One additional factor that may contribute to this trend is the amounts of *c*-planes exposed on the surface of the mesocrystals. Note that the *c*-planes of ZnO have been demonstrated to be a superior facet in photocatalytic activity.[13] Recall that the mesocrystal structure became more porous and elongated in the *c*-axis at low Tris concentrations, because of the looser and less perfect packing of the primary nanocrystals *via* weaker OA. This would cause more exposure of the *c*-planes through staggering of adjacent nanocrystals along the *c*-axis. If the effect of the sample surface area is taken into account, *i.e.*, taking the specific surface area normalized specific rate constant as the photocatalytic activity measure,[14] the ZnO mesocrystals obtained at 100 mM of Tris showed comparable photocatalytic activity as that of P-25 TiO_2, with a normalized specific rate constant value of 28.3 *vs.* 28.9 of P-25.

4. Conclusions

In conclusion, we have developed an ultrafast, green, facile, and effective antisolvent approach for preparation of ZnO mesocrystals. The as-synthesized mesocrystal products exhibited excellent photocatalytic activities toward photodegradation of MB, comparable to that of P-25 TiO_2, which is rarely achieved for pristine ZnO. The feasibility of the present antisolvent approach toward large-scale production of ZnO mesocrystals shall foster further interest to investigate their practical applications in technologically important areas such as photovoltaics, energy storage, chemical sensing, and chemical catalysts. The present approach is a general one and can be readily extended to production of mesocrystals of other functional metal oxides.

Acknowledgements

This work was supported by the National Science Council of the Republic of China (Taiwan) under grants NSC-98-2213-M-009-015-MY2 (Y.-J.H.), NSC-97-2221-E-007-049 (D.S.-H.W.), and NSC-98-2221-E-007-034-MY3 (S.-Y.L.).

References

1 R. Q. Song and H. Cölfen, *Adv. Mater.*, 2010, **22**, 1301.
2 L. C. Soare, P. Bowen, J. Lemaitre and H. Hofmann, *J. Phys. Chem. B*, 2006, **110**, 17763.
3 C. Zhang, J. Chen, Y. C. Zhou and D. Q. Li, *J. Phys. Chem. C*, 2008, **112**, 10083.
4 S. Wohlrab, N. Pinna, M. Antonietti and H. Cölfen, *Chem.–Eur. J.*, 2005, **11**, 2903.
5 D. D. Medina and Y. Mastai, *Cryst. Growth Des.*, 2008, **8**, 3646.
6 J. X. Fang, B. J. Ding, X. P. Song and Y. Han, *Appl. Phys. Lett.*, 2008, **92**, 173120.
7 J. X. Fang, B. J. Ding and X. P. Song, *Cryst. Growth Des.*, 2008, **8**, 3616.
8 J. Y. Feng, M. C. Yin, Z. Q. Wang, S. C. Yan, L. J. Wan, Z. S. Li and Z. G. Zou, *CrystEngComm*, 2010, **12**, 3425.
9 Z. H. Li, A. Geßner, J. P. Richters, J. Kalden, T. Voss, C. Kübel and A. Taubert, *Adv. Mater.*, 2008, **20**, 1279.
10 A. P. Abbott, G. Capper, D. L. Davies, R. K. Rasheed and P. Shikotra, *Inorg. Chem.*, 2005, **44**, 6497.
11 J. Y. Dong, Y. J. Hsu, D. S. H. Wong and S. Y. Lu, *J. Phys. Chem. C*, 2010, **114**, 8867.
12 X. B. Wang, W. P. Cai, Y. X. Lin, G. Z. Wang and C. H. Liang, *J. Mater. Chem.*, 2010, **20**, 8582.
13 A. McLaren, T. Valdes-Solis, G. Q. Li and S. C. Tsang, *J. Am. Chem. Soc.*, 2009, **131**, 12540.
14 S. M. Chang, P. H. Lo and C. T. Chang, *Appl. Catal., B*, 2009, **91**, 619.

